ACS OMEGA

Open Access

http://pubs.acs.org/journal/acsodf

Article

Chitosan-Derived Nitrogen-Doped Carbon as a Support of Cobalt(II)-Phthalocyanine/Gold Nanoparticles for Photocatalytic Water Splitting

Sajjad Keshipour* and Faezeh Eyvari-Ashnak

Cite This: *ACS Omega* 2023, 8, 41624–41632

Read Online

ACCESS | Metrics & More | Article Recommendations

ABSTRACT: Water splitting is considered one of the worthy approaches to generate hydrogen as a green fuel with diverse applications. Promoting this reaction with the photocatalytic strategy enjoys a free source of solar energy, without the use of expensive instruments. In this research, gold nanoparticles and cobalt(II)-phthalocyanine were deposited on nitrogen-doped carbon, obtained from chitosan, to afford a photocatalytic water splitting at the rate of 792 mol mol_{Au}^{-1} h^{-1}. Gold as the catalyst in contact with cobalt(II)-phthalocyanine as the sensitizer and nitrogen-doped carbon as the support/semiconductor provided a desired heterojunction for the photocatalytic purpose. The nanocomposite showed remarkable light harvesting in the region of visible light with a band gap of 2.01 eV. While a facile protocol to the synthesis of the mentioned photocatalyst by a simple thermal treatment of cobalt(II)-phthalocyanine and chitosan could be invaluable, this research pointed out the significance of cobalt(II)-phthalocyanine as the sensitizer in the gold photocatalytic transformations.

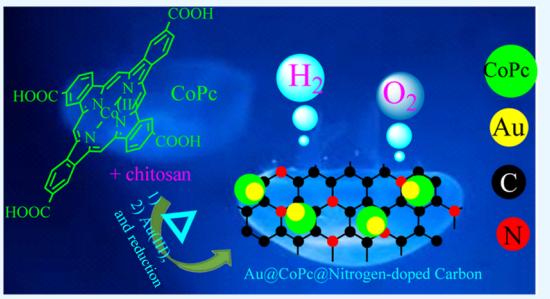

INTRODUCTION

Chitosan gained a broad range of applications due to the some special features such as ecofriendly nature, abundancy, low cost, easy manipulation, high content of nitrogen, and insolubility in most of the solvents.[1] This biopolymer could be the fascinating precursor for the synthesis of nitrogen-doped carbon (NC) by a thermal decomposition reaction because it could provide both nitrogen and carbon atoms for the construction.[2−7] This facile, effective, and inexpensive pathway provides NC for various purposes, in particular, it generates an optically active support for the photocatalysts.[8] The obtained NC has some characteristics such as strongly anchoring to the transition metals, high optical activity, generating n-type semiconductor, and sustainability.[9−13] This kind of semiconductor easily retards charge recombination due to the presence of nitrogen atoms, which leads to the durability of the photocatalyst.[14] Moreover, abundance of nitrogen atoms in the chitosan structure leads to the high content of this atom in the synthesized NC, which in turn affords remarkable active sites to the deposition of transition metals.[15,16] NC is considered a promising support for the photocatalytic hydrogen generation since protons easily are promoted to H_2 after binding to the nitrogen.[17] Considering the mentioned advantages, NC is one of the powerful supports for photocatalysts, and chitosan is a valuable source for its production.

Phthalocyanines (Pcs) are macrocyclic compounds with remarkable optical activities arisen from their structures, including an extended conjugated π-system constructed from carbon and nitrogen atoms.[18] It is worthy to note that, Pcs also have broad absorptions in both UV and Vis regions, by which high-performance semiconductors have been synthesized.[19] Furthermore, Pc possesses a convenient center for placing a metal, leading to the additional activity of the material for the catalytic agenda. These optical and catalytic activities of metallophthalocyanines have led to significant applications of them in the photocatalytic processes like photocatalytic hydrogen generation both as a sensitizer or photocatalyst.[20] Cobalt(II)-*Pc* (CoPc) has promoted various photocatalytic reactions; among them, hydrogen generation is considered as the invaluable reaction for the green energy contributions.[17,21−24]

Pollution released from fossil fuels threaten the environment and humanity by creating substantial climate changes. Hydrogen is one of the potent candidates to save the world possessing green nature, high energy content, and easy production.[25] Therefore, improving efficient approaches for hydrogen generation is the center of attention, in which the photocatalytic

Received: August 7, 2023
Revised: October 6, 2023
Accepted: October 10, 2023
Published: October 25, 2023

https://doi.org/10.1021/acsomega.3c05801
ACS Omega 2023, 8, 41624−41632

pathways are considered as the promising ones, enjoying low energy consumption, easy handling (opposite to the electrochemical methods), and facile synthesis.[26−30] Impressive efforts have been paid to the designing photocatalysts with a dominant focus on enhancing semiconductor operations by decreasing the band gap and increasing absorption.[31] Herein, Au@CoPc@NC was easily synthesized by the thermal treatment of CoPc and chitosan to afford CoPc@NC in a one-pot reaction and subsequent deposition of gold nanoparticles (NPs) (Scheme 1). The main core idea is designing a photocatalyst with a lower

Scheme 1. Synthesis of Au@CoPc@NC

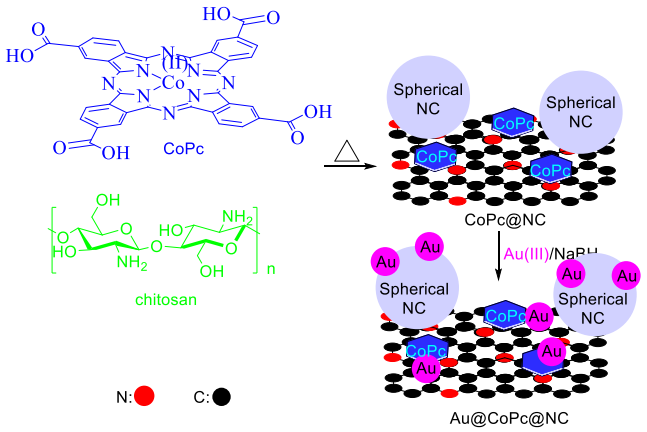

band gap, higher absorption, and remarkable catalytic activity by a simple protocol. We believed that the establishment of a *Z*-scheme heterojunction between NC/CoPc could boost the performance of gold. Concurrently with this research, the synergistic effect of Co-porphyrin and gold was reported, in which the gold supported on Co-5,10,15,20-meso-tetrakis(4-pyridyl)porphyrin was employed in the hydrogen generation.[32] While this nanocomposite had superior light harvesting potential and high catalytic activity, some significant issues could be considered, including the expensive nature of the used porphyrin, instability of gold NPs on porphyrin, and trouble in recovery of the photocatalyst. Au@CoPc@NC stay away from these concerns by the use of cost-effective CoPc and large NC sheets which enjoy the assured supporting gold and easy recovery. In the meantime, the high number of nitrogen atoms in NC enhances the charge transfer and retards their recombination. It is worthy to note that the nitrogen atoms of NC also facilitate hydrogen evolution reaction by decreasing the activation energy.[17] Analyses on the photocatalyst also demonstrated the formation of spherical NC on the sheets.

EXPERIMENTAL SECTION

Materials and Synthesis. Reagents of Sigma-Aldrich and chitosan (80−90% deacetylated, 161.n MW) of Golden-shell Biochemical Co., Ltd. (Zhejiang, China) were used without further purification.

Synthesis of Au@CoPc@NC. Chitosan (4 g) was dissolved in acetic acid (100 mL, 5 wt %) and mixed by a stirrer to give a hydrogel during 4 h. Tetracarboxylic acid-CoPc (0.5 g) was added to the vessel, and stirring was continued for 2 h. The temperature of the mixture was increased up to 100 °C, and mixing was followed to completely remove the solvent. Next, the obtained solid was heated under a N_2 atmosphere at 250 °C for 2 h. Then, the resulting dark solid was dispersed in NaOH solution (0.1 M) and sonicated for 10 min. The solid was filtered off, and the residue was washed with acetone (3 × 10 mL) and dried in an oven at 60 °C to yield 1.73 g of CoPc@NC. $HAuCl_4$ solution (0.12 M, 0.1 mL) was poured to 10 mL of H_2O, and then, 2 g of CoPc@NC was added. The resulting mixture after 30 min sonication in water bath was treated by $NaBH_4$ solution (10 wt %) under vigorous stirring at room temperature until quenching the bubbling. On completion of the reduction of gold, the dark solid was separated by filtration, washed with deionized water (3 × 10 mL), and dried in an oven at 60 °C to afford Au@CoPc@NC (1.9 g).

Characterization. SEM micrographs of FESEM TESCAN MIRA3 and high-resolution transmission electron microscopy (HRTEM) images of an FEI Tecnai G^2 F20 SuperTwin TEM with a 200 kV field emission gun were employed. Co and gold determinations were done by an inductively coupled plasma (ICP) mass spectrometry. Fourier transform infrared (FT-IR) spectroscopy of the AVATAR FTIR instrument of Thermo company in the range of 500−4000 cm^{-1} and Raman spectroscopy of RENISHAW Raman provided the required data. X-ray photoelectron spectroscopy (XPS) was carried out by FlexPS equip (Specs) with a monochromatic Al K_α ($h\nu$ = 1486.6 eV) source, 100 W power, and 10 kV voltage. Diffractograms of an X-ray diffraction (XRD) Philips type PW1730 goniometer at 40 kV were analyzed by Cu K_α radiation (λ = 1.540598 Å) in the 2θ range of 10−90° with a scan rate of 0.05° per second. UV−vis spectra were recorded by a WPA Biowave LifeScience UV−vis spectrometer using quartz cuvettes with a path length of 0.01 m in H_2O as the solvent. AUTOLAB PGSTAT 30 equipment conducted cyclic voltammetry (CV) by three electrodes containing modified GCE (2 mm diameter) as a working electrode in 5 mL of 0.5 M KCl, Ag/AgCl (1 M KCl) as reference electrode, and platinum wire as the auxiliary electrode in the potential region of −0.8 to 1.5 V at a scan rate of 50 mV s^{-1}.

Typical Procedure for Water Splitting. Photocatalytic activity of Au@CoPc@NC for the water splitting was conducted by a 200 W xenon lamp (λ > 420 nm) for 20 mL of distilled water in the presence of various amounts of the photocatalyst. The reaction examined in a vessel connected by a hose to a reversed buret filled with water to trap the generated gases.[26−31] To run the reaction, a mixture of 0.04 g of Au@CoPc@NC in 20 mL of distilled water was stirred at room temperature in a dark room to obtain well dispersion, and then, the light was powered on. The calculations for the volume of H_2 were performed assuming both H_2 and O_2 act as ideal gases.

RESULTS AND DISCUSSION

To confirm the loading CoPc on NC, the FT-IR spectrum of CoPc@NC was provided and compared with the spectra of CoPc and chitosan. The chitosan spectrum showed peaks ascribed to stretching modes of NH/OH (3434 cm^{-1}), stretching modes of CH (2929 and 2850 cm^{-1}), and bending mode of NH (1627 cm^{-1}). With the calcination of chitosan to NC, all of the mentioned peaks were shifted, approving the transformation. Moreover, a new peak also appeared in the spectrum of CoPc@NC at 1714 cm^{-1}, which was also observed in the spectrum of CoPc. This peak attributed to the C═O of CoPc, a confirmation for CoPc contribution in the final product structure. For a more precise study of the transformation of chitosan to NC, the Raman spectrum was provided for CoPc@NC, in which peaks observed at 1361 and 1572 cm^{-1} attributed to the D-band (bending of CH) and G-band (stretching of C═

https://doi.org/10.1021/acsomega.3c05801
ACS Omega 2023, 8, 41624−41632

C), respectively, approving formation of the carbon material.[4] The low intensity of the D-band compared to the G-band also confirms the low number of hydroxyl groups on the produced structure. Furthermore, the D + G-band was also observed at 2919 cm^{-1} related to the stretching modes of CH groups. Generation of NC could also be deduced from the diffractogram obtained from XRD spectroscopy by observing (002) and (101) peaks (Figure 1C).[5] The broad (002) peak of NC at 2Θ ~ 20°

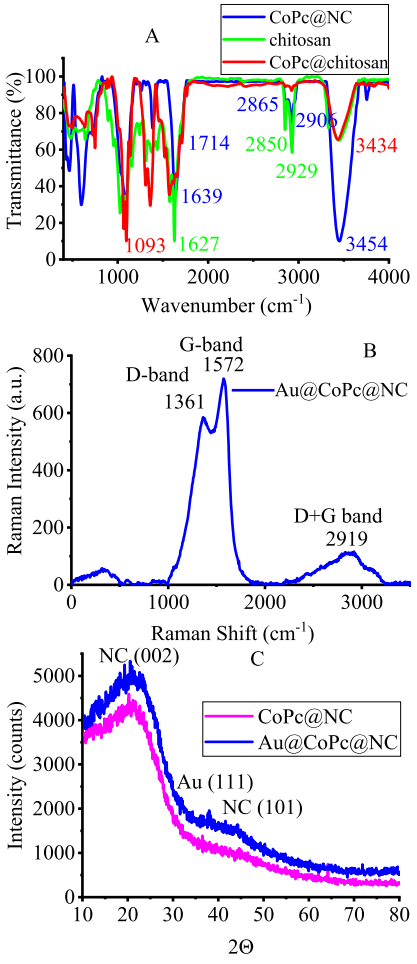

Figure 1. FT-IR spectra (A), Raman spectrum (B), and XRD diffractograms (C) prepared from the synthesized samples.

covered the CoPc peak at about 25°, requiring more analysis to show CoPc such as XPS. The XRD pattern also demonstrated (101) of gold NPs at 2Θ = 38.1°.[29] The broadening of this peak says about the fine sizes of gold NPs.

Au@CoPc@NC was analyzed by XPS to determine the ingredients, oxidation numbers, and types of bonds. This characterization indicated all of the expected atoms, including C, O, N, Co, and Au (Figure 2). Deconvolutions on Au peaks indicated Au 4f7/2 at 84.6 eV and 4f5/2 at 87.9 eV, revealing the formation of gold NPs.[33] It is worthy to highlight that the absence of the peak at about 90 eV confirms complete reduction of Au(III) (Figure 2A). An expansion in the carbon region showed various types of bonding among carbon, nitrogen, and oxygen species (Figure 2B). The nitrogen atoms generated photoelectrons ascribed to amine and imine bonds (Figure 2C). Peaks of 397.5, 398.7, and 401.6 are attributed to the pyridinic, pyrrolic, and quaternary bonds, a sign to an amorphous structure and formation of abundant edges.[34] Finally, the cobalt(II) peaks at 779.9 and 794.8 belong to the CoPc deposited on NC (Figure 2E).[17]

The FESEM micrograph showed formation of coarse spherical particles, deposited on a support. The elemental mapping showed these paricles as the worthy platform for the subsequent Au NPs deposition (Figure 3). As can be seen from the elemental mapping, the concentration of Au NPs on these spherical particles was higher than other sites. This was also observable from the FESEM image, where the high content of heavy atoms on these particles led to their shining (Figure 3A) To find out the exact nature of these spherical NPs, they were observed with an HRTEM instrument (Figure 3C,D). The micrographs showed particles with a size of about 130 nm (Figure 3C), which focused on a gold-free region of this NP at the edge and demonstrated an amorphous structure belonging to NC (Figure 3D). The preference of gold NPs to perch on the spherical amorphous NC could be attributed to the fine size of NC, which acted as the nucleation seeds. Considering this fact, the spherical amorphous carbon will be the most significant site for the hydrogen evolution in water splitting. The loading amounts of gold NPs on the CoPc@NC was determined 1.1 w % by the ICP−MS.

To characterize the gold NPs, HRTEM of the nanocomposite was provided, in which NPs with the broad range of sizes were observed (Figure 4A,B). To reveal the nature of the NPs, the high angle annular dark field (HAADF) of the sample was obtained, and elemental mapping was done on the revealed NPs (Figure 4C,D). These analyses showed that gold atoms contributed in the construction all of the spherical nanoparicles, in which these particles are the result of deposition of gold atoms on CoPc. To approve this, the EDS analysis also was conducted by HRTEM which showed the elements of all ingredients, in particular, Co and Au as the most important species to approve the presence of CoPc and gold NPs, respectively (Figure 4E). The crystalline Au particles were also verified with selected area electron diffraction (SAED) images with observing planes of (111), (200), (220), and (311) (Figure 4F).

The optical activity of the synthesized nanocomposite was studied by UV−vis spectroscopy to determine the range of photoabsorption, band gap energy, and highest occupied molecular orbital−lowest unoccupied molecular orbital (HOMO−LUMO) energies. The UV−vis spectrum showed broad absorptions for Au@CoPc@NC in both UV and Vis regions ascribed to CoPc with Soret-band in UV−vis and Q-band in Vis areas.[28] The remarkable potential of the photocatalyst in light absorption was a prelude for initiating a photocatalytic process. Moreover, the band gap energy was calculated by drawing a Tauc plot, a powerful pathway for this determination. As can be seen from Figure 5B, the band gap energy obtained as 2.01 eV, which is a low value for a photocatalyst, offered excitation with low energy photons. To calculate the LUMO energy level, CV was carried out on the sample, afforded the reduction peak at 1.09 eV. With respect to the equation $E_{HOMO} = -(E_{ox} + 4.75)$, the value of E_{HOMO} was obtained as −5.84 eV. With the addition of the band gap energy to E_{HOMO}, the value of E_{LUMO} was calculated as −3.83 eV (Figure 3C).[17] To reveal the impact of NG on the photoactivity of the Au@CoPc@NC composite, the UV−vis spectrum and Tauc plot of CoPc were provided, in which Au@CoPc@NC was obtained with a band gap energy of 2.01 eV. This finding demonstrates that the photoactive part of the Au@CoPc@NC was CoPc. CV of CoPc showed a significant decrease in the

https://doi.org/10.1021/acsomega.3c05801
ACS Omega 2023, 8, 41624−41632

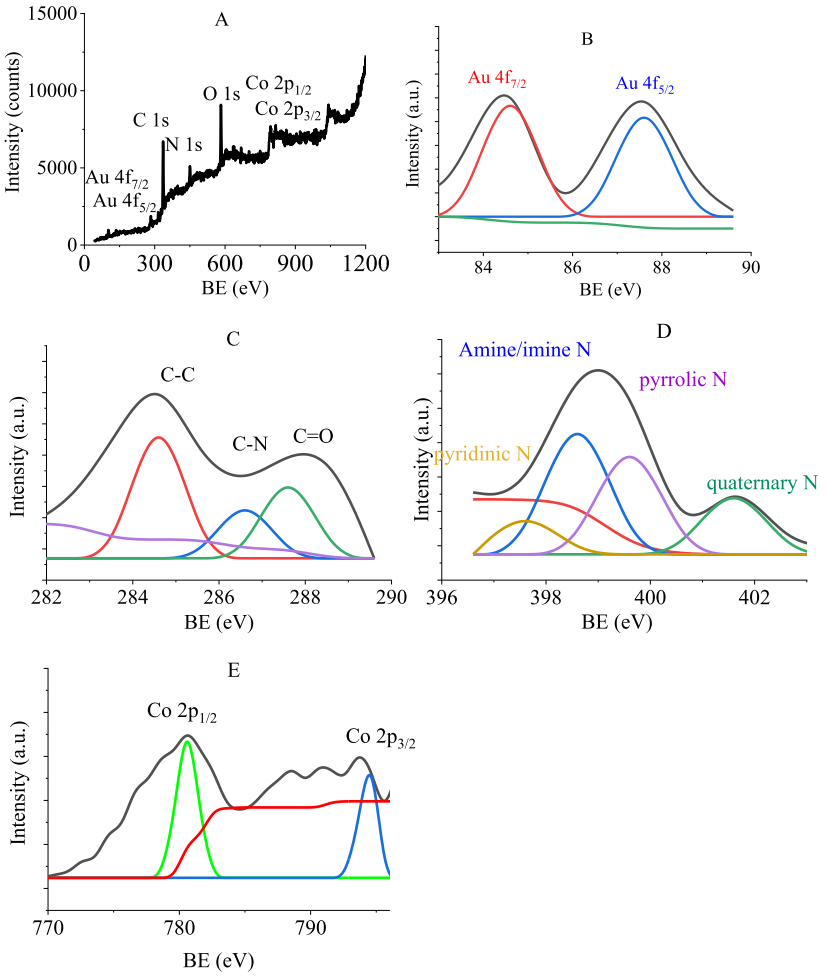

Figure 2. XPS of Au@CoPc@NC (A) and deconvolution of Au (B), carbon (C), nitrogen (D), and CoPc (E).

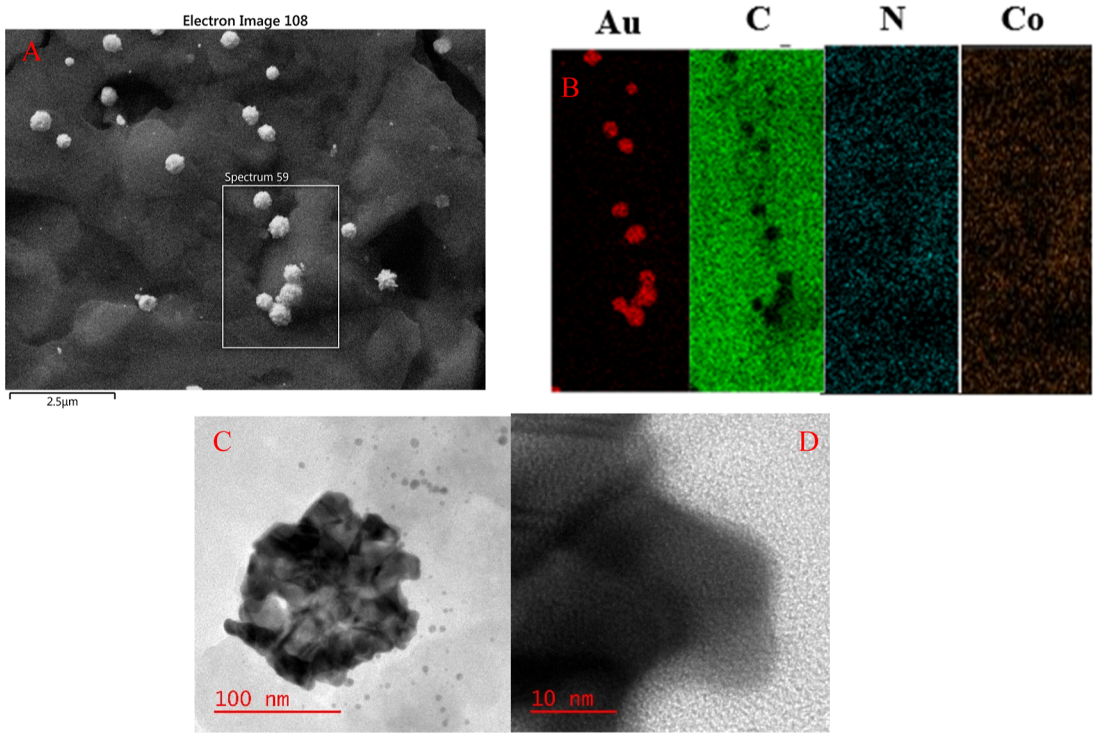

Figure 3. FESEM image (A), elemental mapping (B), and HRTEM images (C,D) of Au@CoPc@NC.

https://doi.org/10.1021/acsomega.3c05801
ACS Omega 2023, 8, 41624−41632

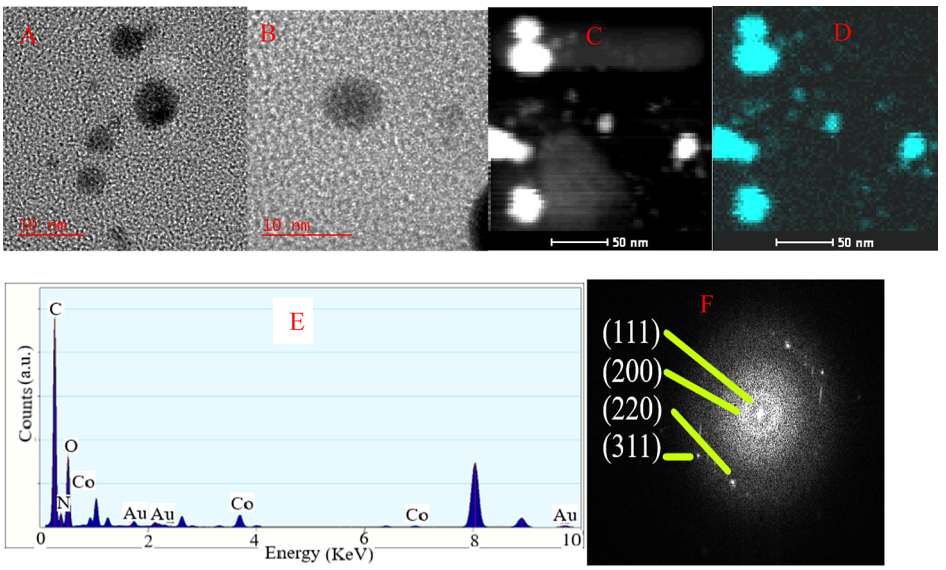

Figure 4. HRTEM images (A,B), HAADF (C,D), elemental mapping (E), and SAED (F) of Au@CoPc@NC.

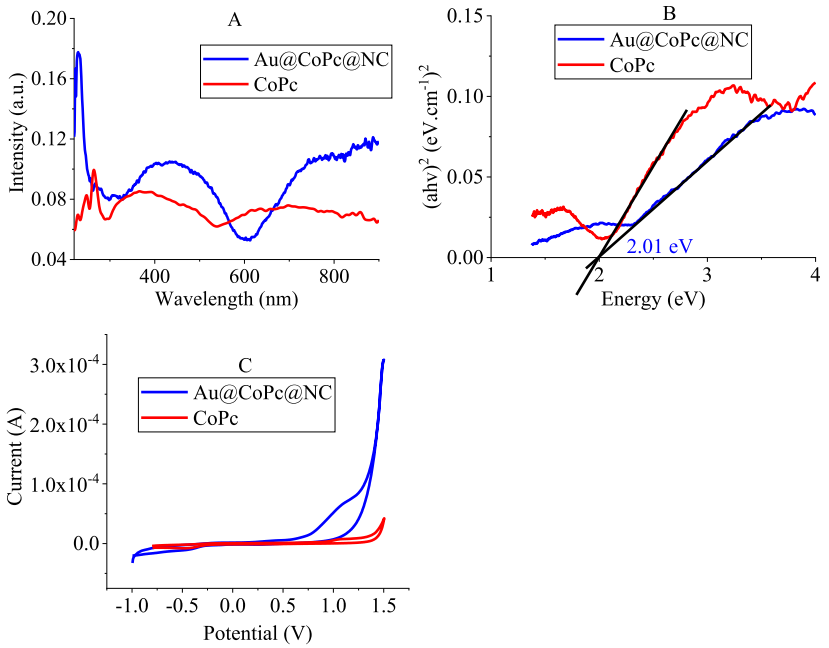

Figure 5. UV−vis spectra (A), Tauc plots (B), and CVs (C) of Au@CoPc@NC and CoPc.

current compared to that of Au@CoPc@NC, revealing the effect of support in the enhancing electron transfer.

The photocatalytic activity of Au@CoPc@NC was evaluated in the water splitting reaction to optimize the reaction conditions. First and foremost, the photocatalyst amounts were optimized by running the reaction with various amounts of Au@CoPc@NC at room temperature (Figure 6A). The minimum amount of Au@CoPc@NC for generating a maximum value of hydrogen was recognized as 0.02 g (Figure 6A). This photocatalyst afforded a hydrogen generation rate of 792 mol mol_{Au}^{-1} h^{-1} during 10 min, where a decrease in the overall rate was observed with the increase in the catalyst. The loaded amounts of Au influenced the hydrogen evolution rate with an optimized amount of 0.8 wt % of the photocatalyst (Figure 6B). Hydrogen generation was screened during the time for 1 h, in which a decrease in the photocatalytic activity of Au@CoPc@NC was observed after 10 min (Figure 6C). It is worthy to note that the decline in the gas production rate over the time was attributed to the aggregation of gold NPs as will bestudied in continue. The value of pH could impress the water splitting rate since the acidic and basic conditions facilitate hydrogen evolution and oxygen generation reactions, respectively. Therefore, the reaction was examined in pHs of 4.5 and 9.5, in which the best results were observed in acidic conditions, a little better than natural pH (Figure 6D). A low difference between the yields obtained in natural and acidic conditions convinced us to consider the natural one as the main reaction since it enjoys additive-free opportunity. The power of lamp was substantial impact on the reaction, following the equation $Y = 3.69P + 54$ (Figure 6E), where P is the power of lamp as W, and Y is the rate of the produced gas as μmol g^{-1} h^{-1}. The effect of temperature also showed a harmonic relation with the generated volume of

https://doi.org/10.1021/acsomega.3c05801
ACS Omega 2023, 8, 41624−41632

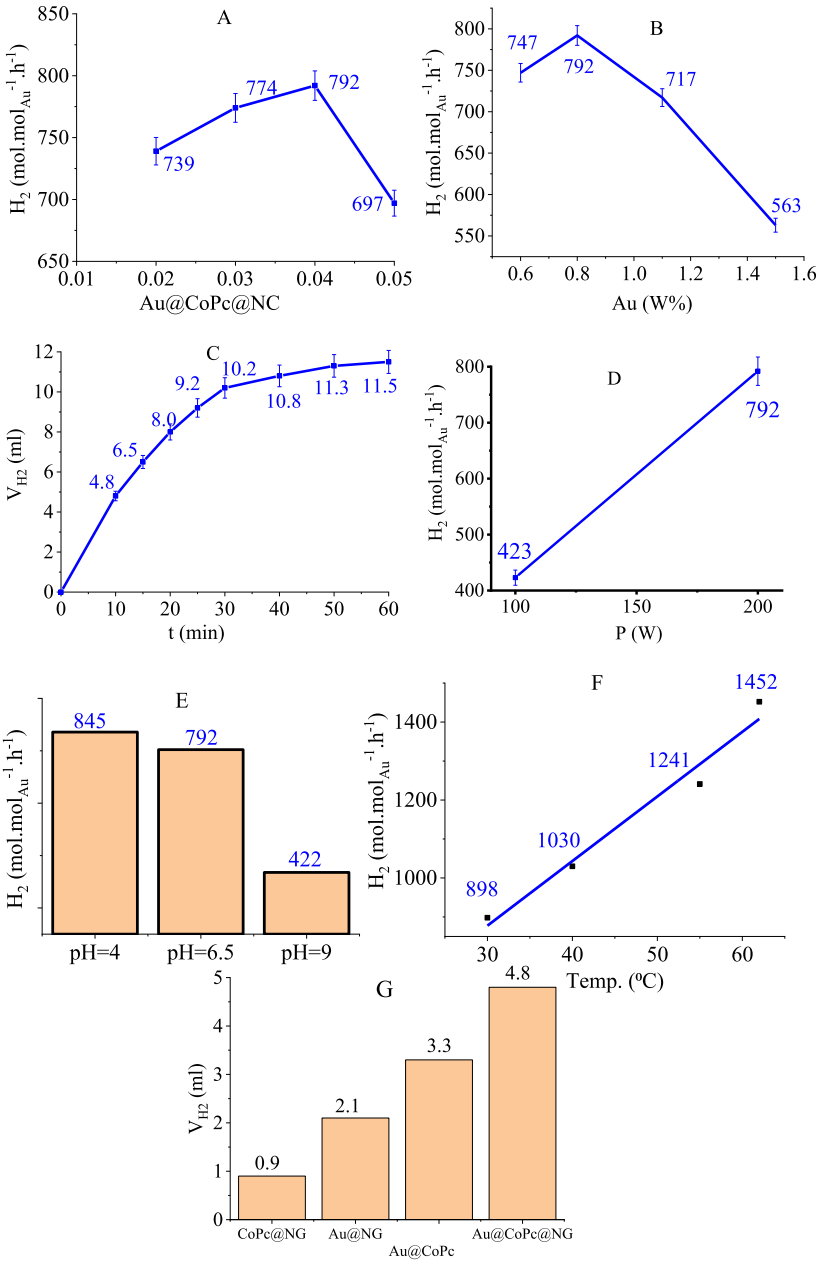

Figure 6. Effects of photocatalyst amount (A), Au amount (B), time (C), lamp power (D), pH (E), temperature (F), and kind of photocatalyst (G) on the reaction yield.

gas as $Y = 16.573T + 380.45$ (Figure 6F), where T is the temperature as °C, and Y is the rate of the produced gas as $mol.mol_{Au}^{-1}.h^{-1}$. This study also revealed an activation energy of 10.83 KJ mol^{-1} for this reaction by the Arrhenius equation. To reveal the roles of photocatalysts ingredients on the reaction, results of hydrogen generation by a similar mol ratio of Au@CoPc@NC, CoPc@NC, Au@NC, and Au@CoPc are summarized in Figure 6G. Significant findings in this stage were the synergistic effect of Au and CoPc to obtain the highest yield and the role of NG to promote the reaction with lowest amounts of Au and CoPc.

The hot filtration test could reveal the reaction phase by removing the photocatalyst in the middle of the reaction. With separation of Au@CoPc@NC after 10 min from the beginning, the gas production was stopped, proof for the reaction taking place on the photocatalyst surface. Moreover, the ICP spectroscopy on the filtrate of the reaction did not show any Au and Co. This test also confirmed the stability of the Au and CoPc on NC, ascribed to (i) in situ deposition of CoPc on NC, which provides strong interaction between support-CoPc and (ii) stability of Au NPs on the nitrogen-enriched support in additive-free media. Some analyses were carried out on recovered Au@CoPc@NC to evaluate its changes during the reaction. The FT-IR spectrum of the recovered photocatalyst did not indicate any significant changes as can be seen from Figure 7A. The TEM image of the recovered Au@CoPc@NC confirmed the stability of the NPs on the photocatalyst, although some aggregations occurred on the surface of the photocatalyst (Figure 7B). As mentioned above, these aggregations are in charge of reducing the reaction rate in long times.

A mechanism was proposed for the water splitting reaction according to the formation of the Z-scheme heterojunction

https://doi.org/10.1021/acsomega.3c05801
ACS Omega 2023, 8, 41624−41632

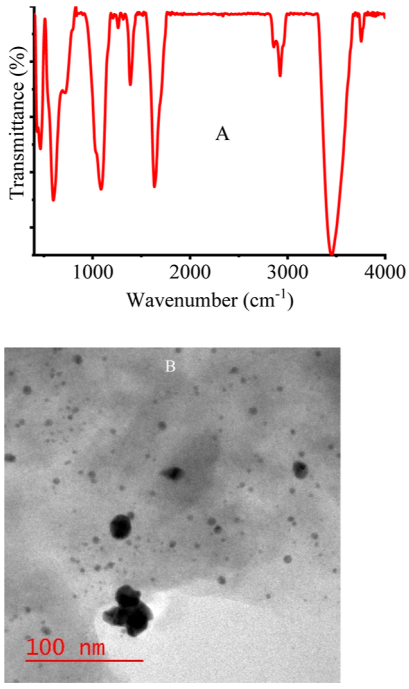

Figure 7. FT-IR spectrum (A) and TEM image of the recovered Au@CoPc@NC (B).

between gold with NC and CoPc (Scheme 2).[35,36] CoPc and NC generate electron/hole pairs with the irradiation, where the

Scheme 2. Proposed Mechanism for Water Splitting by Au@CoPc@NC

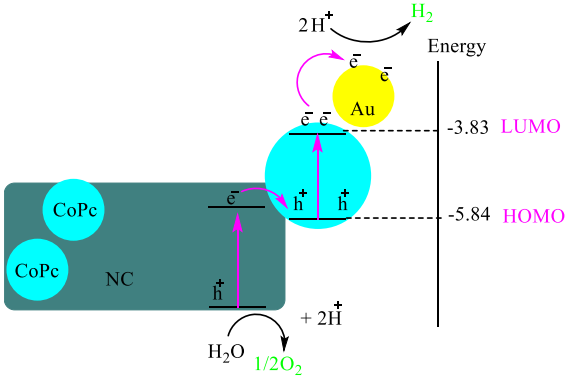

produced electrons were transferred onto the gold NPs, and holes were consumed in the evolution of the O_2 evolution. Creation of a *Z*-scheme type heterojunction elevates the reaction rate since the moving electrons onto gold NPs prevent them from charge recombination. Moreover, gold as a conductor as well as a catalyst could easily move electrons on its surface to be consumed in the H_2 evolution.

A comparison was carried out with the previous related reports regarding yields and reaction conditions. Au@CoPc@NC showed better performance than both photocatalysts based on gold (Table 1, entries 1[37] and 2[38]) and CoPc (Table 1, entries 3[39] and 4[40]). Although high catalytic activity of gold was reported in this area,[41] this comparison approves synergistic effects of gold and CoPc in the hydrogen generation reaction. Moreover, CoPc@NC also indicated better performance compared to CoPc-based photocatalysts, confirming the vital

Table 1. Comparison of the Results of Water Splitting by Various Photocatalysts

entry	photocatalyst	H_2 generation rate (μmol g^{-1} h^{-1})
1	glutathione-capped gold nanoclusters[37]	300
2	gold−ZnSe[38]	437.8
3	CoPc-25/Sn−C[39]	636.99
4	CoPc/TiO2[40]	1051
5	Au@CoPc@NC	19,800
6	CoPc@NC	2008

role of NC in this reaction. NC elevates the rate of hydrogen evolution by both charge recombination retardation and light absorption enhancement. Finally, recyclability for several times, ecofriendly nature, easy synthesis, and remarkable capability of light harvesting in the broad range of the safe region are other advantages of Au@CoPc@NC. It is worthy to highlight that CoPc is an economical catalyst than the close structures like porphyrins with superior performance in hydrogen generation.[42,43]

CONCLUSIONS

A triple-system nanocomposite was designed to be employed in water splitting to hydrogen generation including NC, CoPc, and gold. The synthesis section of this study pointed out an efficient strategy for loading CoPc on NC by a simple thermal treatment of a chitosan/CoPc mixture via a one-pot process. It should be highlighted that chitosan is an invaluable starting material for the facile construction of NC. In the characterization of the synthesized nanocomposite, the absorption in a broad range of UV−vis was observed and ascribed to the presence of CoPc. It seems that CoPc could be employed to enhance the photoharvesting ability of many of the photocatalysts. Finally, in the application of the nanocomposite, the synergistic effect of CoPc and gold was observed in the water splitting to afford the rate of hydrogen generation of 792 mol mol_{Au}^{-1} h^{-1}. A *Z*-scheme type of heterojunction between the ingredients led to significant activity of the photocatalyst, offering the composite of gold/CoPc as a promising combination for the photocatalytic agenda. The inexpensive nature of CoPc, and its easy scale up, are advantages that preferred use of this compound compared to derivative of porphyrin discussed before.

AUTHOR INFORMATION

Corresponding Author

Sajjad Keshipour − *Department of Nanotechnology, Faculty of Chemistry, Urmia University, Urmia 57179-44514, Iran;* orcid.org/0000-0001-7306-6455; Email: s.keshipour@urmia.ac.ir

Author

Faezeh Eyvari-Ashnak − *Department of Nanotechnology, Faculty of Chemistry, Urmia University, Urmia 57179-44514, Iran*

Complete contact information is available at: https://pubs.acs.org/10.1021/acsomega.3c05801

Author Contributions

Sajjad Keshipour: data curation; funding acquisition; investigation; project administration; resources; software; supervision; validation; visualization; writing original draft; and

https://doi.org/10.1021/acsomega.3c05801
ACS Omega 2023, 8, 41624−41632

writing review and editing. **Faezeh Eyvari-Ashnak**: data curation; formal analysis; investigation; methodology; resources; software; validation; and visualization.

Notes

The authors declare no competing financial interest.

■ ACKNOWLEDGMENTS

We gratefully acknowledge financial support from the Research Council of Urmia University. We gratefully acknowledge Electron Microscope Center of Urmia University for the TEM service.

■ REFERENCES

(1) Al-Azmi, A.; Keshipour, S. Cross-linked chitosan aerogel modified with Pd(II)/phthalocyanine: Synthesis, characterization, and catalytic application. *Sci. Rep.* **2019**, *9* (1), 13849.
(2) Malini, K.; Selvakumar, D.; Kumar, N. S. Nitrogen doped activated carbon derived from chitosan/hexamethylenetetramine: structural and CO_2 adsorption properties. *J. Porous Mater.* **2022**, *29* (5), 1539−1550.
(3) Prasanna, K.; Subburaj, T.; Jo, Y. N.; Santhoshkumar, P.; Karthikeyan, S. K. S. S.; Vediappan, K.; Gnanamuthu, R. M.; Lee, C. W. Chitosan complements entrapment of silicon inside nitrogen doped carbon to improve and stabilize the capacity of Li-ion batteries. *Sci. Rep.* **2019**, *9* (1), 3318.
(4) Wang, X.; Pan, H.; Lin, Q.; Wu, H.; Jia, S.; Shi, Y. One-Step Synthesis of Nitrogen-Doped Hydrophilic Mesoporous Carbons from Chitosan-Based Triconstituent System for Drug Release. *Nanoscale Res. Lett.* **2019**, *14* (1), 259.
(5) Xu, D.; Lu, Y.; Liu, L.; Lu, F.; Zhu, M. Preparation of Nitrogen-Doped Carbon Materials Based on Chitosan for Acetylene Hydrochlorination. *ChemistrySelect* **2022**, *7* (11), No. e202104556.
(6) Zeng, Y.; Cao, H.; Jia, W.; Min, Y.; Xu, Q. An eco-friendly nitrogen doped carbon coating derived from chitosan macromolecule with enhanced corrosion inhibition on aluminum alloy. *Surf. Coat. Technol.* **2022**, *445*, 128709.
(7) Zhao, L.; Wang, Y.; Zhao, X.; Deng, Y.; Xia, Y. Facile Synthesis of Nitrogen-Doped Carbon Quantum Dots with Chitosan for Fluorescent Detection of Fe3+. *Polymers* **2019**, *11* (11), 1731.
(8) Khan, A.; Goepel, M.; Colmenares, J. C.; Gläser, R. Chitosan-Based N-Doped Carbon Materials for Electrocatalytic and Photocatalytic Applications. *ACS Sustain. Chem. Eng.* **2020**, *8* (12), 4708−4727.
(9) Zhang, Y.; Lu, L.; Zhang, S.; Lv, Z.; Yang, D.; Liu, J.; Chen, Y.; Tian, X.; Jin, H.; Song, W. Biomass chitosan derived cobalt/nitrogen doped carbon nanotubes for the electrocatalytic oxygen reduction reaction. *J. Mater. Chem. A* **2018**, *6* (14), 5740−5745.
(10) Chen, R.; Liu, G.; Sun, X.; Cao, X.; He, W.; Lin, X.; Liu, Q.; Zhao, J.; Pang, Y.; Li, B.; Qin, A. Chitosan derived nitrogen-doped carbon dots suppress osteoclastic osteolysis via downregulating ROS. *Nanoscale* **2020**, *12* (30), 16229−16244.
(11) Chauhan, A.; Banerjee, A.; Kar, A. K.; Srivastava, R. Metal-Free N-Doped Carbon Catalyst Derived from Chitosan for Aqueous Formic Acid-Mediated Selective Reductive Formylation of Quinoline and Nitroarenes. *ChemSusChem* **2022**, *15* (23), No. e202201560.
(12) Yang, C.; Zhao, T.; Pan, H.; Liu, F.; Cao, J.; Lin, Q. Facile preparation of N-doped porous carbon from chitosan and NaNH2 for CO_2 adsorption and conversion. *Chem. Eng. J.* **2022**, *432*, 134347.
(13) Rybarczyk, M. K.; Cysewska, K.; Yuksel, R.; Lieder, M. Microporous N-Doped Carbon Obtained from Salt Melt Pyrolysis of Chitosan toward Supercapacitor and Oxygen Reduction Catalysts. *Nanomaterials* **2022**, *12* (7), 1162.
(14) Al-Hajri, W.; De Luna, Y.; Bensalah, N. Review on Recent Applications of Nitrogen-Doped Carbon Materials in CO_2 Capture and Energy Conversion and Storage. *Energy Technol.* **2022**, *10* (12), 2200498.
(15) Chang, D. W.; Baek, J.-B. Nitrogen-Doped Graphene for Photocatalytic Hydrogen Generation. *Chem.—Asian J.* **2016**, *11* (8), 1125−1137.
(16) Keshipour, S.; Eyvari-Ashnak, F. Nitrogen-Doped Electrocatalysts, and Photocatalyst in Water Splitting: Effects, and Doping Protocols. *Chemelectrochem* **2023**, *10* (7), No. e202201153.
(17) Eyvari-Ashnak, F.; Keshipour, S. Amines functionalities on chitosan boasting photocatalytic activity of cobalt(II)-phthalocyanine in water-splitting. *Mol. Catal.* **2023**, *534*, 112820.
(18) Luck, R. A Review of: "Phthalocyanine Materials Synthesis, Structure and Function. *Mater. Manuf. Process.* **1999**, *14*, 450−451.
(19) Bahluli, R.; Keshipour, S. Microcrystalline cellulose modified with Fe(II)− and Ni(II)−phthalocyanines: Syntheses. characterizations, and catalytic applications. *Polyhedron* **2019**, *169*, 176−182.
(20) Keshipour, S.; Asghari, A. A review on hydrogen generation by phthalocyanines. *Int. J. Hydrogen Energy* **2022**, *47* (26), 12865−12881.
(21) Chen, L.; Sagar, R. U. R.; Chen, J.; Liu, J.; Aslam, S.; Nosheen, F.; Anwar, T.; Hussain, N.; Hou, X.; Liang, T. Cobalt phthalocyanine as an efficient catalyst for hydrogen evolution reaction. *Int. J. Hydrogen Energy* **2021**, *46* (37), 19338−19346.
(22) Cp, K. P.; Aralekallu, S.; Sajjan, V. A.; Palanna, M.; Kumar, S.; Sannegowda, L. K. Non-precious cobalt phthalocyanine-embedded iron ore electrocatalysts for hydrogen evolution reactions. *Sustain. Energy Fuels* **2021**, *5* (5), 1448−1457.
(23) Kudrik, E.; Makarov, S.; Ageeva, E.; Dereven'kov, I. Cobalt Phthalocyanine − an Effective Catalyst of Hydrogen Production from Formic Acid. *Macroheterocycles* **2009**, *2*, 69−70.
(24) Giddaerappa; Manjunatha, N.; Shantharaja; Hojamberdiev, M.; Sannegowda, L. K. Tetraphenolphthalein Cobalt(II) Phthalocyanine Polymer Modified with Multiwalled Carbon Nanotubes as an Efficient Catalyst for the Oxygen Reduction Reaction. *ACS Omega* **2022**, *7* (16), 14291−14304.
(25) Ishaq, H.; Dincer, I.; Crawford, C. A review on hydrogen production and utilization: Challenges and opportunities. *Int. J. Hydrogen Energy* **2022**, *47* (62), 26238−26264.
(26) Al-Azmi, A.; Keshipour, S. Carbon-Doping as Efficient Strategy for Improving Photocatalytic Activity of Polysilicon Supported Pd in Hydrogen Evolution from Formic Acid. *Polymers* **2021**, *13* (22), 3919.
(27) Keshipour, S.; Mohammad-Alizadeh, S. Nickel phthalocyanine@graphene oxide/TiO_2 as an efficient degradation catalyst of formic acid toward hydrogen production. *Sci. Rep.* **2021**, *11* (1), 16148.
(28) Keshipour, S.; Mohammad-Alizadeh, S.; Razeghi, M. H. Copper phthalocyanine@graphene oxide as a cocatalyst of TiO2 in hydrogen generation. *J. Phys. Chem. Solids* **2022**, *161*, 110434.
(29) Mousavi-Salehi, S.; Keshipour, S.; Ahour, F. Gold supported on graphene oxide/silica photocatalyst for hydrogen generation from formic acid. *J. Phys. Chem. Solids* **2023**, *176*, 111239.
(30) Al-Azmi, A.; Keshipour, S. New bidental sulfur-doped graphene quantum dots modified with gold as a catalyst for hydrogen generation. *J. Colloid Interface Sci.* **2022**, *612*, 701−709.
(31) Lakhera, S. K.; Rajan, A.; T.P, R.; Bernaurdshaw, N. A review on particulate photocatalytic hydrogen production system: Progress made in achieving high energy conversion efficiency and key challenges ahead. *Renew. Sustain. Energy Rev.* **2021**, *152*, 111694.
(32) Sheng, H.; Wang, J.; Huang, J.; Li, Z.; Ren, G.; Zhang, L.; Yu, L.; Zhao, M.; Li, X.; Li, G.; Wang, N.; Shen, C.; Lu, G. Strong synergy between gold nanoparticles and cobalt porphyrin induces highly efficient photocatalytic hydrogen evolution. *Nat. Commun.* **2023**, *14* (1), 1528.
(33) de Souza Rodrigues, M. P.; Dourado, A. H. B.; Cutolo, L. . d.O.; Parreira, L. S.; Alves, T. V.; Slater, T. J. A.; Haigh, S. J.; Camargo, P. H. C.; Cordoba de Torresi, S. I. Gold−Rhodium Nanoflowers for the Plasmon-Enhanced Hydrogen Evolution Reaction under Visible Light. *ACS Catal.* **2021**, *11* (21), 13543−13555.
(34) Lee, J.; Kim, N.; Shin, D. Y.; Park, H.-Y.; Lee, S.-S.; Joon Kwon, S.; Lim, D.-H.; Bong, K.; Son, J.; Kim, J. Nitrogen-doped graphene-wrapped iron nanofragments for high-performance oxygen reduction electrocatalysts. *J. Nanopart. Res.* **2017**, *19*, 98.

https://doi.org/10.1021/acsomega.3c05801
ACS Omega 2023, 8, 41624−41632

(35) Chang, F.; Yang, C.; Wang, X.; Zhao, S.; Wang, J.; Yang, W.; Dong, F.; Zhu, G.; Kong, Y. Mechanical ball-milling preparation and superior photocatalytic NO elimination of Z-scheme Bi12SiO20-based heterojunctions with surface oxygen vacancies. *J. Clean. Prod.* **2022**, *380*, 135167.
(36) Chang, F.; Zhao, S.; Lei, Y.; Peng, S.; Liu, D.-g.; Kong, Y. Ball-milling fabrication of n-p heterojunctions $Bi_4O_5Br_2/\alpha$-MnS with strengthened photocatalytic removal of bisphenol A in a Z-Scheme model. *Sep. Purif. Technol.* **2023**, *304*, 122324.
(37) Chen, Y.-S.; Kamat, P. V. Glutathione-Capped Gold Nanoclusters as Photosensitizers. Visible Light-Induced Hydrogen Generation in Neutral Water. *J. Am. Chem. Soc.* **2014**, *136* (16), 6075−6082.
(38) Chen, W.; Li, X.; Wang, F.; Javaid, S.; Pang, Y.; Chen, J.; Yin, Z.; Wang, S.; Li, Y.; Jia, G. Nonepitaxial Gold-Tipped ZnSe Hybrid Nanorods for Efficient Photocatalytic Hydrogen Production. *Small* **2020**, *16* (12), 1902231.
(39) Lu, M.; Sun, Z.; Zhang, Y.; Liang, Q.; Zhou, M.; Xu, S.; Li, Z. Construction of cobalt phthalocyanine sensitized SnIn4S8/g-C3N4 composites with enhanced photocatalytic degradation and hydrogen production performance. *Synth. Met.* **2020**, *268*, 116480.
(40) Genc, E.; Yüzer, A. C.; Yanalak, G.; Harputlu, E.; Aslan, E.; Ocakoglu, K.; Ince, M.; Patir, I. H. The effect of central metal in phthalocyanine for photocatalytic hydrogen evolution via artificial photosynthesis. *Renewable Energy* **2020**, *162*, 1340−1346.
(41) Chattopadhyay, S.; Sarkar, A.; Chatterjee, S.; Dey, A. Functional adlayers on Au electrodes: some recent applications in hydrogen evolution and oxygen reduction. *J. Mater. Chem. A* **2018**, *6* (4), 1323−1339.
(42) Bhunia, S.; Rana, A.; Hematian, S.; Karlin, K. D.; Dey, A. Proton Relay in Iron Porphyrins for Hydrogen Evolution Reaction. *Inorg. Chem.* **2021**, *60* (18), 13876−13887.
(43) Rana, A.; Mondal, B.; Sen, P.; Dey, S.; Dey, A. Activating Fe(I) Porphyrins for the Hydrogen Evolution Reaction Using Second-Sphere Proton Transfer Residues. *Inorg. Chem.* **2017**, *56* (4), 1783−1793.

https://doi.org/10.1021/acsomega.3c05801
ACS Omega 2023, 8, 41624−41632